https://doi.org/10.20965/jrm.2016.p0273

Paper:

On High-Performance Airfoil at Very Low Reynolds Number

Katsuya Hirata*, **Ryo Nozawa***, **Shogo Kondo***, **Kazuki Onishi***, **and Hirochika Tanigawa****

*Department of Mechanical Engineering, Doshisha University
1-3 Tatara Miyakodani, Kyotanabe, Kyoto 610-0321, Japan
E-mail: khirata@mail.doshisha.ac.jp
**Department of Mechanical Engineering, National Institute of Technology, Maizuru College
234 Shiroya, Maizuru 625-8511, Japan
E-mail: tanigawa@maizuru-ct.ac.jp

[Received November 30, 2015; accepted April 24, 2016]

The airfoil is often used as the elemental device for flying/swimming robots, determining its basic performances. However, most of the aerodynamic characteristics of the airfoil have been investigated at Reynolds numbers Re's more than 10^6. On the other hand, our knowledge is not enough in low Reynolds-number ranges, in spite of the recent miniaturisation of robots. In the present study, referring to our previous findings (Hirata et al., 2011), we numerically examine three kinds of high-performance airfoils proposed for very-low Reynolds numbers; namely, an iNACA0015 (the NACA0015 placed back to front), an FPBi (a flat plate blended with iNACA0015 as its upper half) and an FPBN (a flat plate blended with the NACA0015 as its upper half), in comparison with such basic airfoils as a NACA0015 and an FP (a flat plate), at a Reynolds number $Re = 1.0 \times 10^2$ using two- and three-dimensional computations. As a result, the FPBi shows the best performance among the five kinds of airfoils.

Keywords: low Reynolds number, airfoil, blade, wing, aerodynamics

1. Introduction

The airfoil is one of the most elemental devices for flying/swimming robots to control flow and its reacting force, which determines their basic performances. However, the aerodynamic characteristics of the airfoil have been researched mainly in high Reynolds-number ranges more than 10^6, in a historic context closely related with the developments of airplanes and fluid machineries in the last century [1–4]. On the other hand, we have been requiring more precise knowledge about the aerodynamic characteristics of the airfoil especially in low Reynolds-number ranges less than 10^6, because of the recent miniaturisation of robots such as unmanned aerial vehicles known as UAVs or micro air vehicles known as MAVs [5, 6], in addition to the importance of insect/bird flight dynamics, small-scale machines like micro fluid machineries and micro combustion engines and so on (also, see Subsection 3.1).

Concerning the aerodynamic characteristics at low Reynolds numbers, there have been several studies [7–24]. However, in such low Reynolds number ranges, our knowledge has not been enough yet, due to the laminar-to-turbulent transition with strong nonlinearity which brings us some technical difficulties in the accuracies of analyses, computations and experiments.

Recently, we have investigated such basic two-dimensional airfoils as a NACA0015, a flat plate (hereinafter, referred to as FP) and some flat plates with modified fore-face and back-face geometries at Reynolds numbers Re's $< 1.0 \times 10^5$ using two- and three-dimensional computations together with wind-tunnel and water-tank experiments [20]. As a result, we have revealed the effect of the Reynolds number Re upon the minimum drag coefficient $C_{D\min}$ at $Re = 1.0 \times 10^2$–1.0×10^5 about two kinds of basic airfoils. Besides, at $Re = 1.0 \times 10^2$, we have shown the effects of attack angle α upon various aerodynamic characteristics such as the drag coefficient C_D, the lift coefficient C_L and the lift-to-drag ratio C_L/C_D, discussing those effects on the basis of both near-flow-field information and surface-pressure profiles. Such results suggest the importance of sharp leading edges, which implies the possibility of an inversed NACA0015 (hereinafter, referred to as iNACA0015). Furthermore, concerning the FP, we have revealed the influences of fore-face and back-face geometries upon such effects.

In the present study, referring to our previous findings [20], we suppose three kinds of two-dimensional airfoils with high performance at very low Re's; namely, the iNACA0015, an FPBi and an FPBN (for their definitions, see later). And we examine them at $Re = 1.0 \times 10^2$ in comparison with such basic airfoils as the NACA0015 and the FP by two- and three-dimensional computations. Specifically speaking, we focus our attention upon the flow at $Re = 1.0 \times 10^2$. Then, we investigate the effects of attack angle α upon various aerodynamic characteristics such as C_D, C_L and C_L/C_D. In order to discuss the revealed α effects, we visualise the flow around the airfoils using the Q value, the helicity, streamlines and pressure/vorticity distributions around the airfoils at

$\alpha = 0°, 4°, 16°$ and $18°$, together with surface-pressure profiles on the airfoils.

Nomenclature

$2A_F$:	flap amplitude (up-to-down) [m]
c :	chord length = characteristic length scale [m]
C_D :	drag coefficient
C_L :	lift coefficient
C_L/C_D :	lift-to-drag ratio
C_p :	pressure coefficient
f_F :	frap frequency [Hz]
H :	physical computational domain size [m]
H_R :	relative helicity $\equiv (\boldsymbol{v}\cdot\boldsymbol{\omega})/(\lvert\boldsymbol{v}\rvert\,\lvert\boldsymbol{\omega}\rvert)$
Ma :	Mach number
Q :	second invariant of velocity gradient tensor [1/s^2]
Re :	Reynolds number $\equiv \rho U_\infty c/\mu$
$Re(V_{WT})$:	Reynolds number based on $V_{WT} \equiv \rho V_{WT} c/\mu$
s :	wing span [m]
t :	flat-plate thickness [m]
t/c :	cross-section ratio
$\boldsymbol{v} = (u, v, w)$:	flow velocity [m/s]
U_∞ :	mean flow velocity of uniform mainstream [m/s]
V_{WT} :	wing-tip velocity (the maximum over one flap) $\equiv 2\pi A_F f_F$ [m/s]
(x,y,z), (ξ,η,z) :	coordinates [m]
α :	attack angle [°]
α' :	corrected α [°]
$\Delta\xi_{\min}$, $\Delta\eta_{\min}$:	minimum grid size [m]
ρ :	density of fluid [kg/m^3]
μ :	viscosity of fluid [Pa s]
$\boldsymbol{\omega} = (\omega_x, \omega_y, \omega_z)$:	vorticity [1/s]

2. Model

2.1. Model

Figure 1 shows the present models. They are three kinds of two-dimensional airfoils with high performance at low *Re*; namely, an iNACA0015 (the NACA0015 placed back to front), an FPBi (a flat plate blended with the iNACA0015 as its upper half) and an FPBN (a flat plate blended with the NACA0015 as its upper half), together with two kinds of fundamental airfoils such as a NACA0015 and an FP.

All the present five airfoils have a chord length of c. A blended flat plate of the FPBi or the FPBN is a flat plate with a thickness $t/2$. The iNACA0015 and the FPBi resemble the optimum shapes for drag minimisation [18, 19] and for lift maximisation [19], respectively. Both of them are rather the shapes with a sharp edge in front and with a round surface in back.

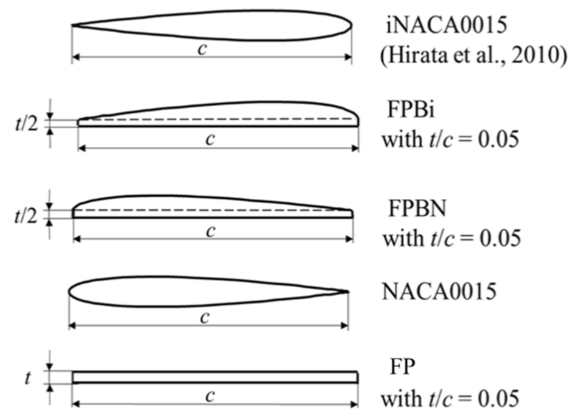

Fig. 1. Models: two-dimensional airfoils.

Concerning the iNACA0015, we have shown the importance of sharp leading edges for the improvement of aerodynamic characteristics at very low *Re*, which bring the sharp and very-low pressure drop near the upper fore-face [22]. This importance of sharp leading edges might imply the iNACA0015.

We also have shown the importances of a non-convex lower surface and a convex upper surface for the improvement [22]. The former brings the lower-surface higher pressure, and the latter brings the slightly-lower pressure widely-distributed over the middle portion of the upper surface at small α. The FPBi is designed, being intended to have sharp edges on its fore-face in addition to a non-convex lower surface and a convex upper surface. The FPBN is designed as well (concerning the importances, also see Subsection 3.5).

The NACA0015 and the FP are two-dimensional airfoils with basic and symmetric cross sections: the NACA0015 is a typical streamlined airfoil for high *Re*, and the FP is the simplest thin airfoil with sharp leading and trailing edges. The FP has a cross-section ratio $t/c = 0.05$.

In order to non-dimensionalise all the concerning physical quantities, we consider c as a characteristic length scale and the mean flow velocity U_∞ of uniform mainstream as a characteristic velocity scale. The tested value of *Re* is fixed to 1.0×10^2 in all the present computations.

2.2. Computational Procedure

We investigate the above five kinds of airfoils, numerically. The present procedure of computation is as well as [22]. In many actual situations, most of the flow at $Re < 10^6$ could be usually regarded as incompressible and viscous. So, we suppose the incompressible full Navier-Stokes equations in three dimensions. We approximately solve the equations by a finite-difference method

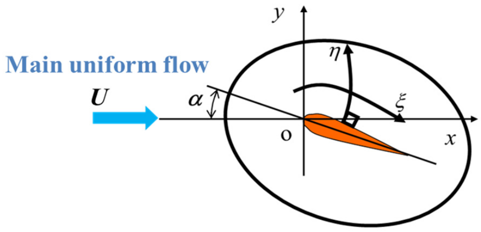

Fig. 2. Model together with a coordinate system. The z-axis is perpendicular to the x-y plane or the ξ-η plane.

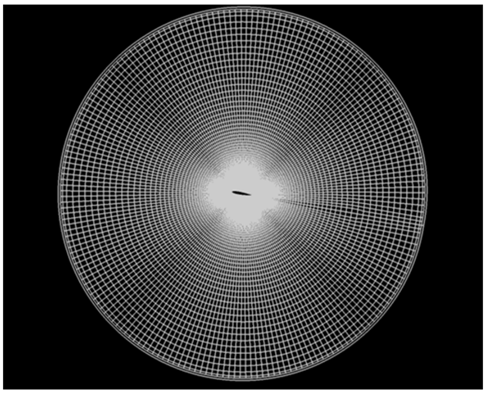

(a) Over-all view: computational domain with a diameter H

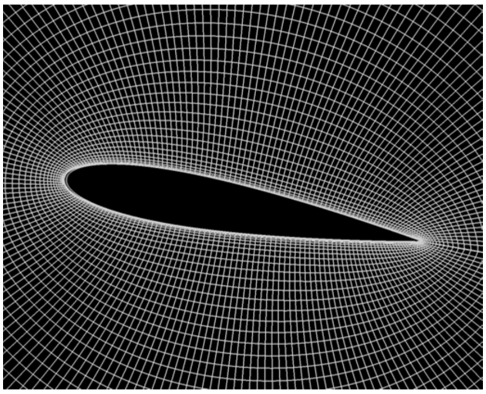

(b) Close-up view: details around an airfoil with minimum grid sizes $\Delta\xi_{\min}$, and $\Delta\eta_{\min}$ on airfoil's surface

Fig. 3. Computational grid on the x-y plane (for NACA0015).

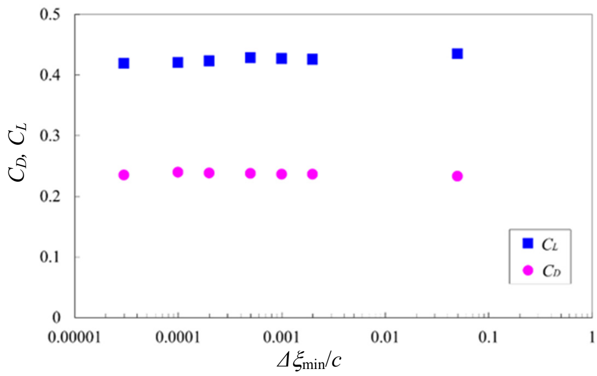

Fig. 4. Influence of the minimum grid size $\Delta\xi_{\min}/c$ in the direction parallel to an airfoil surface (for iNACA0015 at $Re = 1.0 \times 10^2$ and $\alpha = 4°$. with $\Delta\eta_{\min}/c = 0.002$ and $H/c = 28.0$).

using the MAC scheme for velocity/pressure coupling, a third-order-upwind difference scheme in spatial discretisation of convective terms, a second-order-central difference scheme in spatial discretisation of the other terms and the Euler explicit scheme in a time marching.

The boundary condition on the airfoil surface is viscid. On the outer boundaries of the computational domain, we suppose the Dirichlet condition as $u = U_\infty$, $v = 0$ and $w = 0$. As a spatial grid, we use an O-type staggered grid as shown in **Figs. 2** and **3**, which is a boundary-fitted one with a generalised coordinate system (ξ, η). Here, ξ and η represent a tangential and normal coordinates with respect to the airfoil surface, respectively. The grid numbers in the ξ and η directions are 200 and 90, respectively. The minimum grid size $\Delta\eta_{\min}$ is $1.0 \times 10^{-3}c$. And, a physical computational-domain size H is $28.0c$, where H denotes the diameter of a circular computational domain with its origin O at an airfoil's front.

At a time step $\Delta t = 1.0 \times 10^{-4} c/U_\infty$, we proceed with the above time-marching computations, during which we monitor both the values of C_D and C_L, to judge whether the total computation time is enough or not for fully-saturated conditions.

Such parameter values as H, $\Delta\xi_{\min}$, $\Delta\eta_{\min}$ and Δt are determined by many preliminary trials, to achieve negligible influences upon results. **Fig. 4** shows an example of such trials, which represents the influences of $\Delta\xi_{\min}$ upon C_L and C_D for the iNACA0015 at $\alpha = 4°$ with $\Delta\eta_{\min}/c = 0.002$ and $H/c = 28.0$. We can see that both the influences are negligible at $\Delta\xi_{\min}/c \lesssim 0.01$.

3. Results and Discussion

3.1. Flying/Swimming at Low Reynolds Number

At the beginning, we survey the flight/swim of actual creatures in low Re ranges. **Table 1** shows the Reynolds number $Re(V_{WT})$ based on wing-tip velocity V_{WT} of some small animals flying in air at $Re < 10^4$. $Re(V_{WT})$ is defined by $\rho V_{WT} c/\mu$, and V_{WT} is defined by $2\pi A_F f_F$, where ρ, μ, A_F, and f_F are fluid density, fluid viscosity, flap amplitude and flap frequency, respectively. As well, **Table 2** shows $Re(V_{WT})$ of some small animals swimming in water at $Re < 10^3$. **Table 3** shows Re of the plant's seeds gliding in air at $Re \simeq 10^2$–10^3, where a tip rotating speed or a flight speed is used as a characteristic velocity scale.

Figure 5 summarises the relation between Re or $Re(V_{WT})$ and the chord length c for various flying objects in air, namely, some animals flying in air in addition to the MAVs and so on.

We can see that there exit the flights/swims using flapping motion of actual creatures at $Re \simeq 10^2$–10^3. This implies the importance to understand the aerodynamics of airfoils even at such a very low Re as 10^2, although the lift

Table 1. Reynolds number $Re(V_{WT})$ based on wing-tip velocity V_{WT} of the animal's flying in air (at 20°C) at $Re < 10^4$.

	Flap amplitude (up-to-down) $2A_F$ [mm]	Wing span s [mm]	Flap frequency f_F [Hz]	Wing chord (mean) c [mm]	Re (V_{WT})
Fly	0.5-0.7	2-5	600	0.6-0.8	50-200
Mosquito	1.0-1.5	4-6	200	1-2	100-400
Honeybee	2.0-3.0	8-12	200	2-4	500-1000
Butterfly	10-20	30-60	30	10-20	1000-3000
Hummingbird	10-15	40-60	50	10-20	3000-5000

Table 2. Reynolds number $Re(V_{WT})$ based on wing-tip velocity V_{WT} of the animals swimming in water (at 10°C) at $Re < 10^3$.

	flap amplitude (front-to-back) $2A_F$ [mm]	Wing span s [mm]	Flap frequency f_F [Hz]	Wing chord (mean) c [mm]	Re (V_{WT})
Notonecta triguttata (Matsumo-mushi)	3.0-4.0	12-15	2	1	20-60
Clione Pallas	5.0-10	6-12	2	2	70-110
Diving beetle (Gengorou)	5.0-7.0	15-20	3	2	120-160

Table 3. Reynolds number Re of the plant-seed gliding in air (at 20°C) at $Re \approx 10^2$–10^3.

	Wing chord (mean) c [mm]	V_{WT} , U_∞[mm/s]	Re
Maple leaf	10	0.2 (tip rotating speed)	100-200
Alsomitra	7	1.5 (flight speed)	600-800

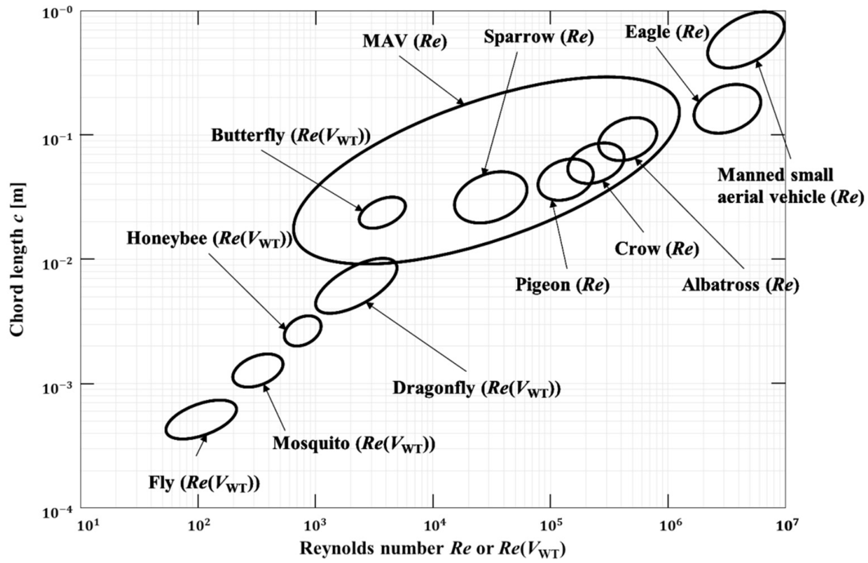

Fig. 5. Relation between Reynolds number Re or $Re(V_{WT})$ and chord length c for various flying objects in air.

force is relatively weakened in comparison with the drag force by strong viscous friction. So, in the following subsection, we restrict our concern into the flow at $Re = 10^2$ as a typical very low Re.

3.2. Two-Dimensionality: Comparison of 2D with 3D

In this subsection, we examine the two-dimensionality of flow concerning the two kinds of airfoils, that is, the iNACA0015 and the NACA0015. More specifically, we

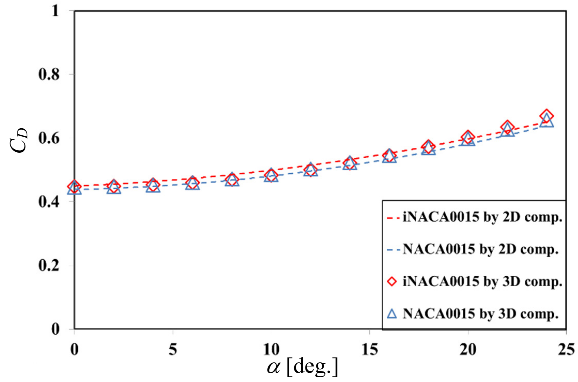

(a) Drag coefficient C_D

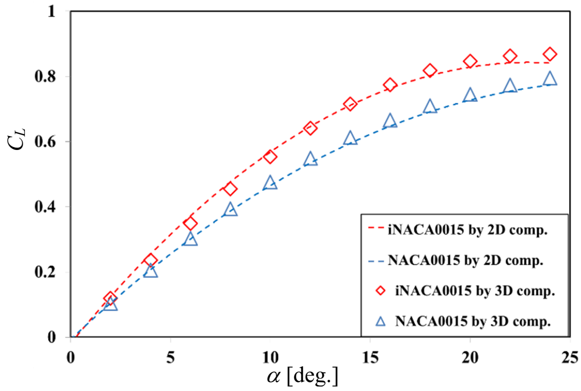

(b) Lift coefficient C_L

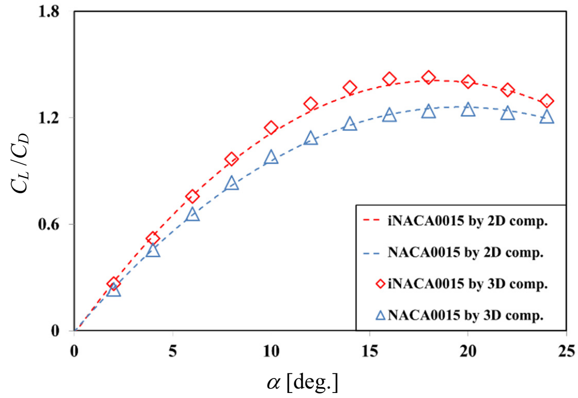

(c) Lift-to-drag ratio C_L/C_D

Fig. 6. Comparison between 2D and 3D computations; aerodynamic characteristics versus attack angle α at $Re = 1.0 \times 10^2$.

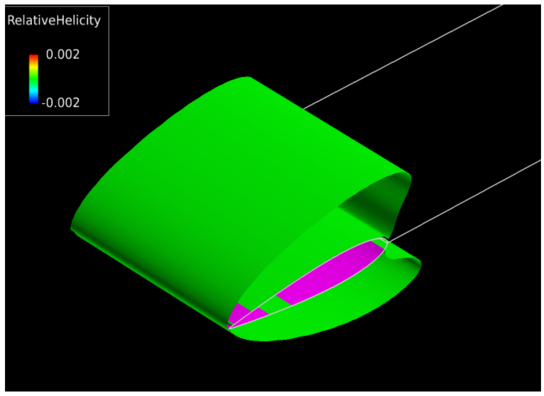

(a) At $\alpha = 4$ deg.

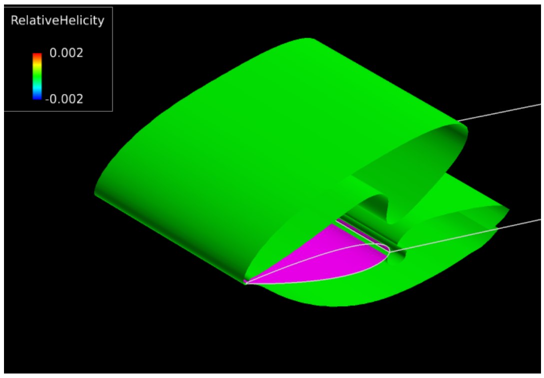

(b) At $\alpha = 18$ deg.

Fig. 7. 3D computation visualised using iso-Q surfaces with a normalised Q value ($\equiv QU_\infty^2/c^2$) of 0.1 (for iNACA0015 at $Re = 1.0 \times 10^2$). The colour on the iso-Q surfaces represents relative helicity He_R shown as a legend on the upper left hand of each figure.

investigate the effects of α upon various aerodynamic characteristics such as the drag coefficient C_D, the lift coefficient C_L and the lift-to-drag ratio C_L/C_D, by means of two-dimensional (hereinafter, referred to as 2D) and three-dimensional (hereinafter, referred to as 3D) computations.

Figure 6 shows the α effects: namely, C_D, C_L and C_L/C_D are plotted against α in **Figs. 6(a)**, **(b)** and **(c)**, respectively. The tested values of α are all positive, because of the symmetry of the airfoils.

When, we compare the results obtained by the 2D computations with those obtained by the 3D computations concerning both the NACA0015 and the iNACA0015, we can confirm good agreement between the 2D and 3D computations, for all the results involving those at such a large α as 24°. This suggests that, at such a low Re as 1.0×10^2, 2D computations are valid to investigate the flow around an airfoil even at large values of α. Then, it can be enough to take account only of 2D computations (for the discussion on aerodynamic characteristics, see Subsection 3.3).

Figures 7 and **8** show samples of 3D computations. More specifically, **Figs. 7** and **8** denote the flows for the iNACA0015 and the NACA0015, respectively. In each figure, **(a)** and **(b)** $\alpha = 4°$ and $18°$, respectively. Both **Figs. 7** and **8** are visualised using iso-Q surfaces with a normalised Q value ($\equiv QU_\infty^2/c^2$) of 0.1. The colour on the iso-Q surfaces represents relative helicity H_R shown as a legend on the upper left hand of each figure. We can see all the flows are fully two-dimensional, because of the tubular shapes of the iso-Q surfaces and because of the value of H_R which is zero everywhere. Besides, we should note that all the tested flows are completely steady.

In summary, the flow at $Re = 1.0 \times 10^2$ is considered to

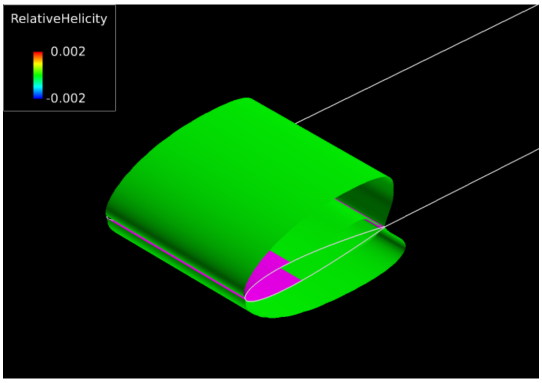

(a) At $\alpha = 4$ deg.

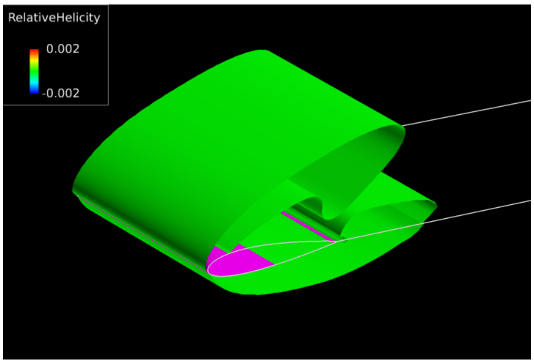

(b) At $\alpha = 18$ deg.

Fig. 8. 3D computation visualised using iso-Q surfaces with a normalised Q value ($\equiv QU_\infty^2/c^2$) of 0.1 (for NACA0015 at $Re = 1.0 \times 10^2$). The colour on the iso-Q surfaces represents relative helicity He_R shown as a legend on the upper left hand of each figure.

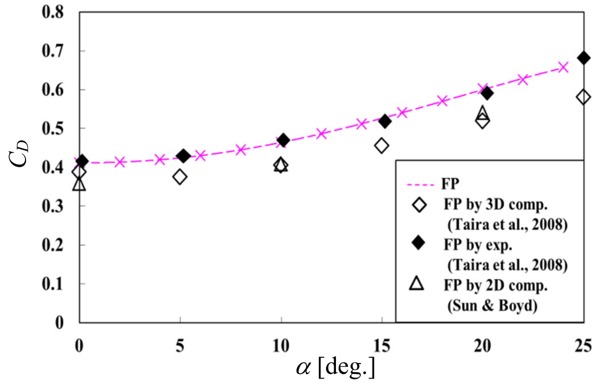

(a) Drag coefficient C_D

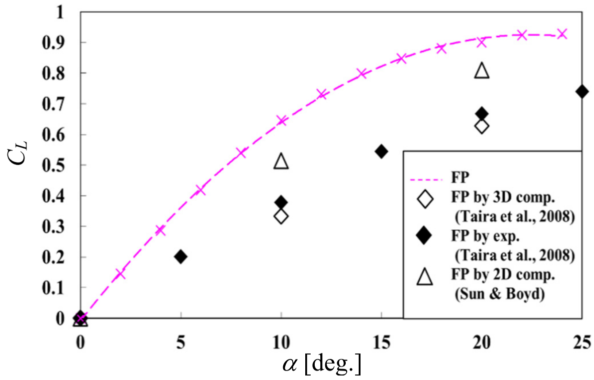

(b) Lift coefficient C_L

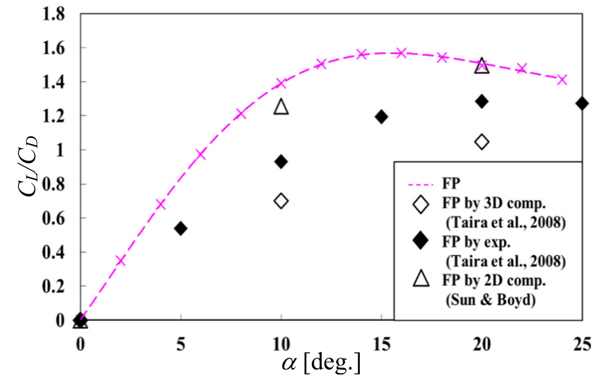

(c) Lift-to-drag ratio C_L/C_D

Fig. 9. Comparison of the present computation for FP to other researchers at $Re = 1.0 \times 10^2$. $\Diamond$, 3D computation by Taira et al. (2008) (for FP with $AR = 2$ and $t/c = 0$ at $Re = 1.0 \times 10^2$). $\blacklozenge$ experiment using oil tow tank by Taira et al. (2008) (for FP with $AR = 2$ and $t/c = 0.037$ at $Re = 1.0 \times 10^2$). $\triangle$, 2D computation by Sun & Boyd (2004) (for FP with $t/c = 0.05$ at $Re = 1.357 \times 10^2$ and $Ma = 0.2$).

be completely steady and two-dimensional even at large α's. So, in the following subsections, we will suppose the two-dimensionality of flow and conduct only 2D computations.

3.3. Aerodynamic Characteristics

At the beginning, we check the present accuracy in computation by comparing to other researchers' results. **Fig. 9** shows the comparison of the present computations for the FP at $Re = 1.0 \times 10^2$ to other researchers: namely, 3D computations by Taira et al. (2008) [21] for the FP with an aspect ratio AR $= 2$ and $t/c = 0.037$ at $Re = 1.0 \times 10^2$ using a grid size of $200 \times 88 \times 128$, experiments using oil tow tank by Taira et al. (2008) [21] for the FP with AR $= 2$ and $t/c = 0.037$ at $Re = 1.0 \times 10^2$, and 2D computations by Sun & Boyd (2004) [15] for the FP with $t/c = 0.05$ at $Re = 1.357 \times 10^2$ and $Ma = 0.2$. Specifically speaking, **Fig. 9** shows the α effects: namely, C_D, C_L and C_L/C_D are plotted against α in **Figs. 9(a)**, **(b)**, and **(c)**, respectively. The tested values of α are all positive, because of the symmetry of the airfoils.

At first, we see our computations of the FP. In **Fig. 9(a)**, C_D monotonically and gradually increases with increasing α in the tested range of $\alpha = 0°$–$24°$. Especially in such a range as $\alpha \lesssim 10°$, C_D can be approximated to a constant value of 0.4. In **Fig. 9(b)**, as α increases from zero, C_L monotonically increases from zero, in the tested range of $\alpha = 0°$–$24°$. More specifically, the increasing rate $dC_L/d\alpha$ of C_L against α is almost constant at small α, but it monotonically reduces with increasing α. Thus, in **Fig. 9(c)**, C_L/C_D monotonically increases with increasing α at $\alpha \lesssim 10°$, as well as C_L. At $\alpha \gtrsim 10°$, the increasing rate $d(C_L/C_D)/d\alpha$ monotonically reduces with increasing α. And at $\alpha = 16°$, $d(C_L/C_D)/d\alpha$ crosses zero toward negative: namely, C_L/C_D attains the maximum at $\alpha = 16°$. Then, a mild stall appears.

Second, we see the other researchers, comparing to the present computations. In summary, we can confirm the accuracy of the present computations which agree well with the other researchers from a qualitative point of view. From a quantitative point of view, there are some discrepancies. That is, C_D, C_L and C_L/C_D by the present computations are in the same orders, but somewhat larger than the other researchers. Among the discrepancies, that between the present computations and Sun & Boyd is the smallest in spite of the difference of *Re*. Larger discrepancies between the present computations and Taira's computations and experiments suggest that the influences of AR are negligible.

Figure 10 summaries the aerodynamic characteristics of the five airfoils at $Re = 1.0 \times 10^2$. The figure shows the α effects: namely, C_D, C_L and C_L/C_D are plotted against α in **Figs. 10(a)**, **(b)** and **(c)**, respectively. The tested values of α are all positive, as well as **Fig. 9**.

In summary, all the aerodynamic characteristics of the five airfoils qualitatively resemble with one another.

At first, we see **Fig. 10(a)**. For all the five airfoils, C_D monotonically and gradually increases with increasing α in the tested range of $\alpha = 0°$–$24°$. Not only qualitatively but also quantitatively, C_D resembles with one another. Then, C_D can be approximated to a constant value of 0.4 in such a range as $\alpha \lesssim 10°$, for all the five airfoils.

Second, we see **Fig. 10(b)**. C_L monotonically increasing α in the tested range of $\alpha = 0°$–$24°$, for the four airfoils except for the iNACA0015 for which C_L attains the maximum at $\alpha = 22°$. On the other hand, the increasing rate $dC_L/d\alpha$ monotonically reduces with increasing α with the constant-$dC_L/d\alpha$ range at small α, for all the five airfoils. From a quantitative point of view, we see obvious discrepancies among the five airfoils, which depend upon α.

Third, we see **Fig. 10(c)**. For all the five airfoils, C_L/C_D monotonically increases with increasing α at $\alpha \lesssim 10°$. At $\alpha \gtrsim 10°$, $d(C_L/C_D)/d\alpha$ monotonically reduces with increasing α. And at a certain α in the range of $\alpha = 16°$–$22°$, $d(C_L/C_D)/d\alpha$ crosses zero toward negative: namely, C_L/C_D attains the maximum at the certain α. Then, a mild stall appears for each airfoil. From a quantitative point of view, we again see obvious discrepancies among the five airfoils, which depend upon α.

If we quantitatively estimate aerodynamic performance more strictly among the five airfoils, **Fig. 10** is not fare. That is to say, C_L and C_L/C_D are not zero at $\alpha = 0$ for both the FPBi and the FPBN because of their non-symmetries. To correct these camber effects of both the airfoils, we introduce another attack angle α' instead of α so as to both C_L and C_L/C_D are zero at $\alpha' = 0$.

Figure 11 shows C_L/C_D plotted against α' at $Re = 1.0 \times 10^2$ in the tested range of α' from $-25°$ to $+25°$. The tested range in the figure is not only positive, as we see non-symmetry in the α'-C_L/C_D relation. Then in

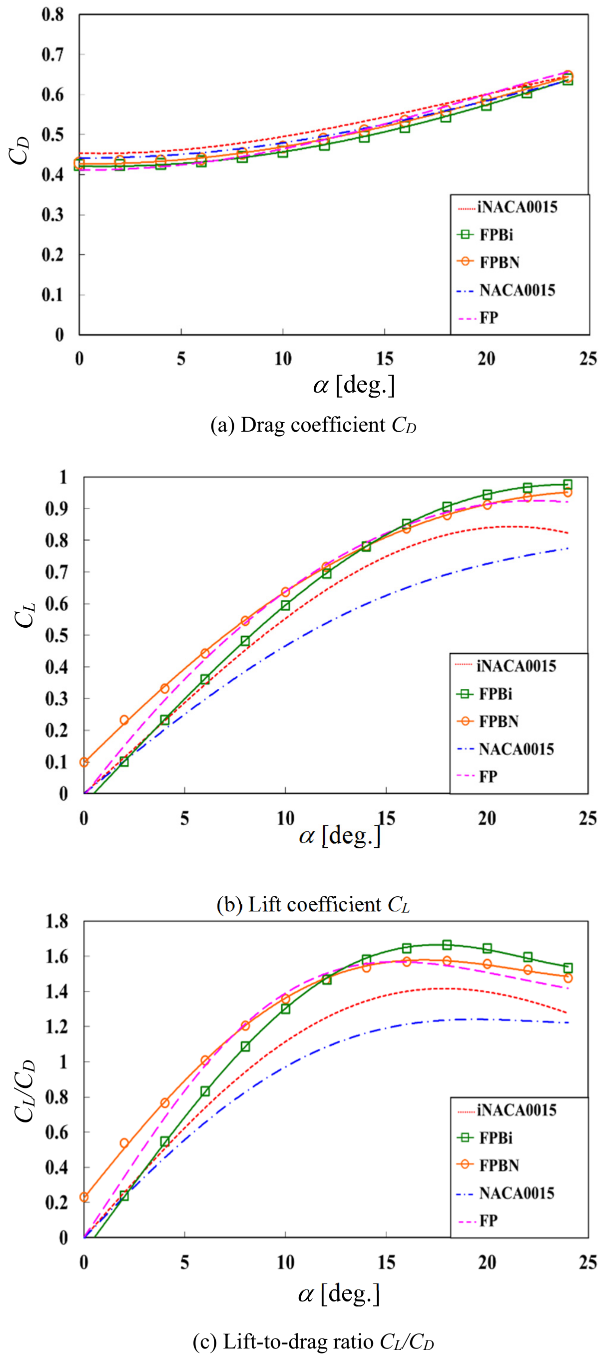

(a) Drag coefficient C_D

(b) Lift coefficient C_L

(c) Lift-to-drag ratio C_L/C_D

Fig. 10. Aerodynamic characteristics versus attack angle α at $Re = 1.0 \times 10^2$.

Fig. 11, as α' increase from zero, C_L/C_D increases from zero for all the five airfoils. And, C_L/C_D attains the maximum at a certain α' for each airfoil, as well as **Fig. 10(c)**.

Now, we compare the performance of the five airfoils on the basis of **Fig. 11**. **Table 4** summarises the results of **Fig. 11**: namely, the maximum values of C_L/C_D for the five airfoils and the corresponding values of α' in addition to their relative improvement to the NACA0015. We can see that the maximum C_L/C_D for the FPBi is the largest among the five airfoils, while such three airfoil as the FPBi, the FPBN and the FP indicate high relative im-

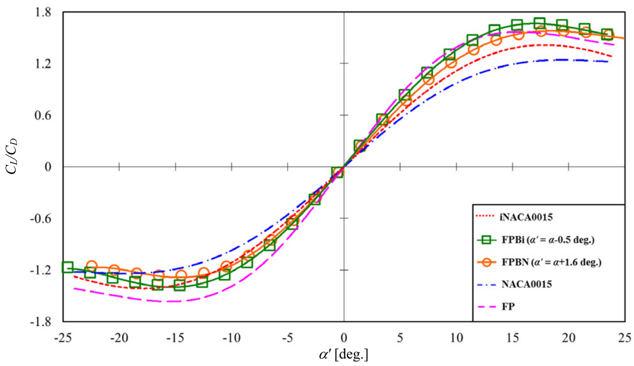

Fig. 11. Lift-to-drag ratio C_L/C_D versus corrected attack angle α' at $Re = 1.0 \times 10^2$ in a range of α' from $-25°$ to $+25°$.

Table 4. Maximum C_L/C_D.

Airfoil	α' (α) [deg.]	C_L/C_D	Relative improvement [%]
iNACA0015	18.0 (18.0)	1.42	14
FPBi	17.5 (18.0)	1.66	34
FPBN	19.6 (18.0)	1.58	27
NACA0015	22.0 (22.0)	1.24	0
FP	16.0 (16.0)	1.59	26

provements larger than 25% in the range of $\alpha' = 15°$–$20°$. The maximum C_L/C_D for the iNACA0015 is smaller than these three best-performance airfoils, but obviously larger than the NACA0015. – For the comparison of those low-Reynolds-number results to such typical high-Reynolds-number ones as Abbott & Doenhoff [2], see [22]. –

In summary, at very low *Re*, the aerodynamic characteristics of the five airfoils are qualitatively similar with one another. And quantitatively, such three airfoils as the FPBi, the FPBN and the FP show the best performance, which are superior to the NACA0015. The aerodynamic performance of the iNACA0015 is between the three best-performance airfoils and the NACA0015. Among the three best-performance airfoils, the FPBi is supreme. Concerning the controllability, the NACA0015 is superior among the five airfoils, due to the lack of a remarkable stall feature on C_L/C_D.

3.4. Flow Visualisation

In this subsection, we consider the flow around an airfoil. – We should note that the flow is at an instance chosen arbitrarily, because all the tested flows at $Re = 1.0 \times 10^2$ are completely steady. – **Figs. 12** and **13** show the visualised flows for the NACA0015 and the FPBi at $Re = 1.0 \times 10^2$, respectively. Specifically speaking, **Figs. 12–13(a)** and **(b)** are at $\alpha = 4°$ and $18°$, respectively. The upper, the middle and the lower cases of each figure represent the pressure distribution, the vorticity distribution and the streamlines around an airfoil, respectively. Pressure p and vorticity ω_z are non-dimensionalised as pressure coefficient C_p and $\omega_z c/U_\infty$, respectively. We indicate the value of C_p or $\omega_z c/U_\infty$ by colour, with its corresponding colour bar on the upper-right hand of each figure. The colour of the streamline indicates the value of $|\boldsymbol{v}|/U_\infty$, with its corresponding colour bar on the upper-right hand of each figure, as well.

At the beginning of this subsection, we summarise the features appearing in both the two reference airfoils like the NACA0015 and the FP [22]. At first, seeing **Fig. 12**, we consider the NACA0015 as one of the two reference airfoils. When we compare a pair of the pressure distributions, namely, the upper cases of **Figs. 12(a)** and **(b)**, we can confirm such similarities as (i) the low pressure widely-distributed over the upstream portion of the upper surface and (ii) the high pressure concentrated just below the fore-face. In addition, we can find slight discrepancies between **Figs. 12(a)** and **(b)**; namely, (iii) the obvious pressure reduction in the widely-distributed low-pressure area over the upstream portion of the upper surface with increasing α, and (iv) the leeward extension of the concentrated high-pressure area just below the fore-face with increasing α. Here, we should note that the peak value of C_p in the concentrated high-pressure area just below the fore-face seems to be independent of α. The two similarities (i) and (ii) and the two slight discrepancies (iii) and (iv) will be quantitatively discussed in **Fig. 14**.

When we compare a pair of the vorticity distributions, namely, the middle cases of **Figs. 12(a)** and **(b)**, we can clearly observe a discrepancy (v) between them. That is to say, we can see the flow separation on the middle upper surface only in **Fig. 12(b)**, not in **Fig. 12(a)**, despite the flow steadiness even in **Fig. 12(b)** and despite the similarities (i) and (ii) between the pressure fields in **Figs. 12(a)** and **(b)**. Respecting the flow visualisation around the NACA0015 at various values of α, we can confirm that this clear discrepancy (v) is connected with both the increasing rates $dC_L/d\alpha$ and $d(C_L/C_D)/d\alpha$ in **Figs. 10(b)** and **(c)**.

We can again observe the clear discrepancy (v), when we compare the streamlines in the lower cases of **Figs. 12(a)** and **(b)**. Specifically speaking, at $\alpha = 18°$ (in **Fig. 12(b)**), we can observe a recirculating-flow area on the downstream portion of the upper surface, together with a flow separation and a flow reattachment on the upper surface. However, at $\alpha = 4°$ (in **Fig. 12(a)**), fluid flows along the airfoil surface without such a recirculating-flow area, and we can observe neither flow separations nor separation bubbles.

Second, we consider the other airfoils. In summary, the above results are the same for the other airfoils except for the iNACA0015 and the FPBi at small α. Then, we show the flow around the FPBi in **Fig. 13**, providing neither the iNACA0015, the FPBN nor the FP. Because the flow around iNACA0015 is almost the same as that around the FPBi, and those around the FPBN and the FP are almost the same as that around the NACA0015.

Only one difference of **Fig. 13** from **Fig. 12** appears in the upper case of **Fig. 13(a)**, where we cannot confirm

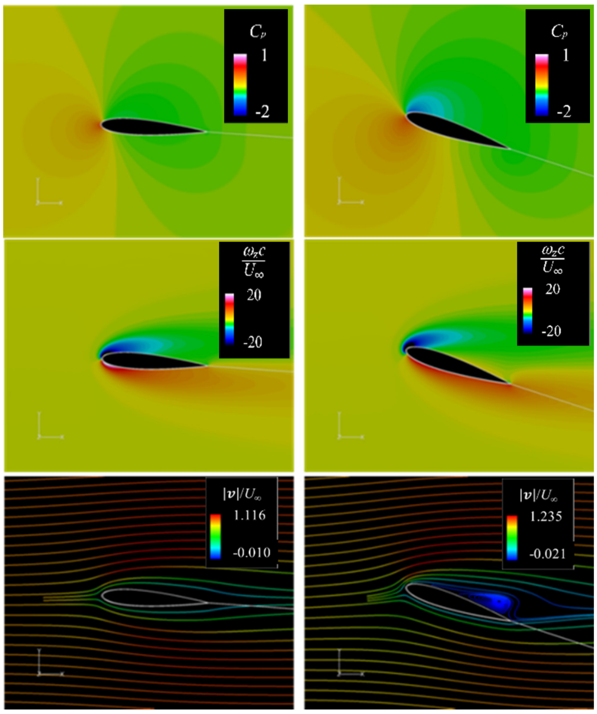

(a) $\alpha = 4$ deg. (b) $\alpha = 18$ deg.

Fig. 12. Pressure distribution, vorticity distribution and streamlines (for NACA0015 at $Re = 1.0 \times 10^2$).

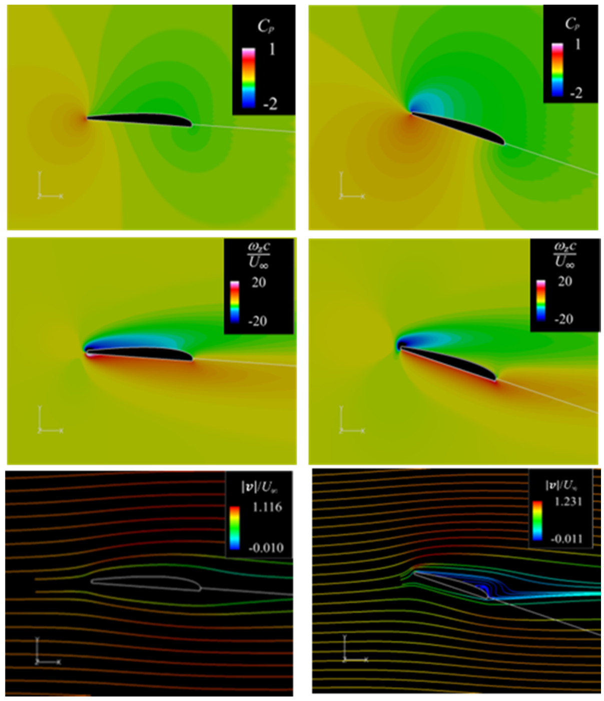

(a) $\alpha = 4$ deg. (b) $\alpha = 18$ deg.

Fig. 13. Pressure distribution, vorticity distribution and streamlines (for FPBi at $Re = 1.0 \times 10^2$).

the similarity (i). Instead, we can confirm (vi) the constant low (but not very low) pressure all over the upper surface. Of course, if we compare a pair of the pressure distributions in the upper cases of **Figs. 13(a)** and **(b)**, we can confirm the other similarity (ii) and the two slight discrepancies (iii) and (iv) as well as the NACA0015. They will also be quantitatively discussed in **Figs. 14–16**. And, if we compare a pair of the vorticity distributions in the middle cases of **Fig. 13** or the streamlines in the lower cases of **Fig. 13** around the FPBi at $\alpha = 4^\circ$ and 18°, we can find the same clear discrepancy (v) in the flow separation on the middle upper surface as the NACA0015. Besides, as well as the NACA0015, respecting the flow visualisations around the FPBi at various values of α, we can confirm that the clear discrepancy (v) is connected both the increasing rates $dC_L/d\alpha$ and $d(C_L/C_D)/d\alpha$.

When we compare the flows of the five airfoils like **Figs. 12** and **13**, it seems consistent that the aerodynamic characteristics of the five airfoils shown in **Fig. 10** are qualitatively similar with one another. Because, for all the five airfoils except for the iNACA0015 and the FPBi at small α, we can confirm all the similarities (i) and (ii), the slight discrepancy (iii) and (iv), and the clear discrepancy (v) which are based on the α effects in the obtained near-flow-field information such as the pressure distribution, vorticity distribution and the streamlines. In the exceptional cases of the iNACA0015 and the FPBi at small α, we can confirm (ii)–(v), together with (vi) instead of (i). However, we cannot discuss the quantitative differences in aerodynamic characteristics between both the airfoils shown in **Fig. 10**, which states the superiority of the FPBi than the other airfoils including the NACA0015. So, we will quantitatively discuss the surface pressure in the following.

3.5. Surface Pressure

Figures 14, **15** and **16** show the surface-pressure profiles at $Re = 1.0 \times 10^2$ on the iNACA0015, the FPBi and the FPBN, respectively, together with both the NACA0015 and the FP for reference. The abscissa x denotes the distance from the leading edge in the leeward direction, which are normalised by c. **Figs. 14–16(a)** and **(b)** are at $\alpha = 4^\circ$ and 18°, respectively.

At the beginning of this subsection, we summarise the features appearing in both the two reference airfoils like the NACA0015 and the FP [22], as well. At first, seeing **Fig. 14**, we consider the NACA0015. In **Fig. 14(a)**, we can confirm the features representing the similarities between $\alpha = 4^\circ$ and 18° such as (i) the widely-distributed low-pressure area over the upstream portion of the upper surface and (ii) the concentrated high-pressure area just below the fore-face. – More minutely, the maximum C_p in the concentrated high-pressure area is much larger than the unity which is common in both the potential theory and high-*Re* experiment, representing a viscosity effect at very-low *Re*. – Of course, when we see **Fig. 14(b)**, we can confirm these features representing the similarities (i) and (ii), as well as **Fig. 14(a)**. In addition, when we compare **Figs. 14(a)** and **(b)**, we can confirm the features representing the slight-discrepancies between $\alpha = 4^\circ$ and 18° such as (iii) the pressure reduction in the widely-distributed

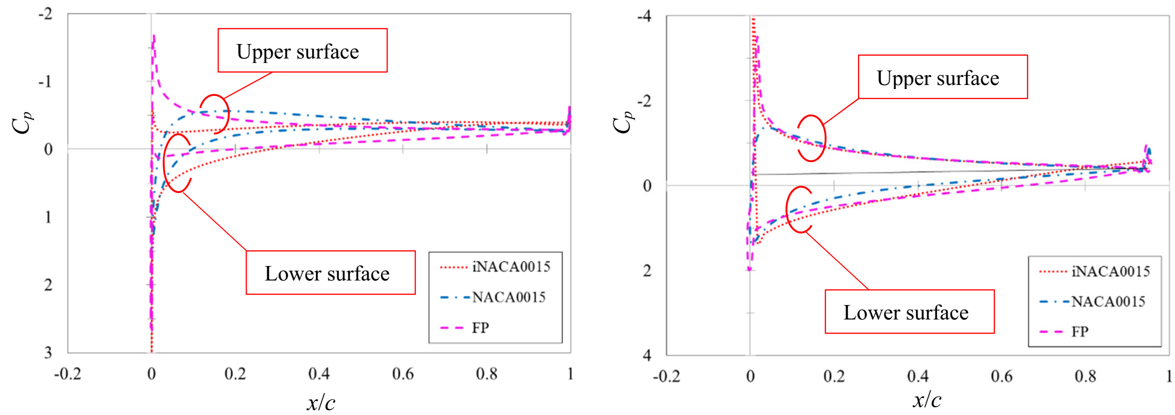

(a) $\alpha = 4$ deg.
(b) $\alpha = 18$ deg.

Fig. 14. Surface-pressure profiles on airfoil surfaces (for iNACA0015 at $Re = 1.0 \times 10^2$).

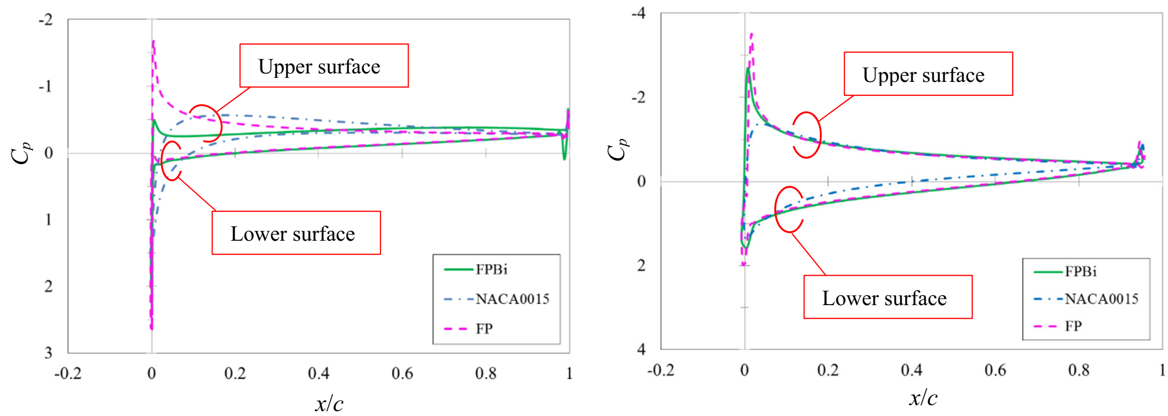

(a) $\alpha = 4$ deg.
(b) $\alpha = 18$ deg.

Fig. 15. Surface-pressure profiles on airfoil surfaces (for FPBi at $Re = 1.0 \times 10^2$).

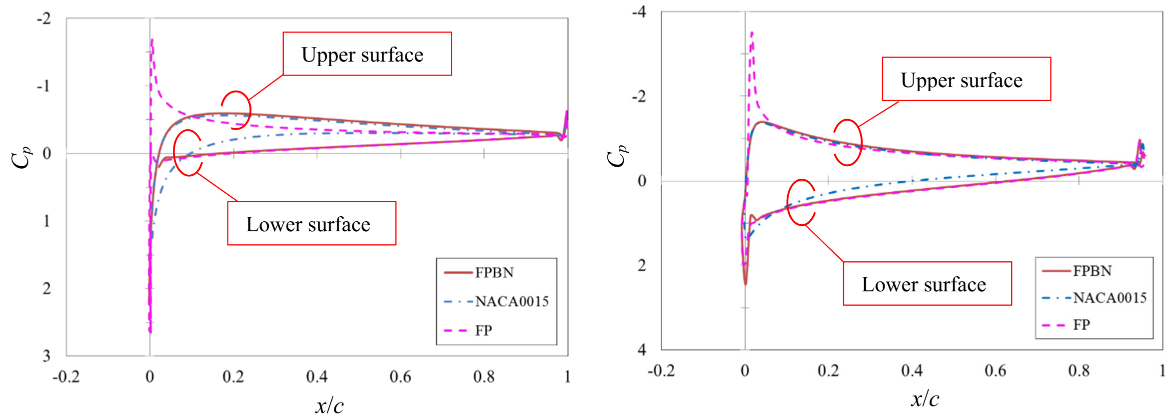

(a) $\alpha = 4$ deg.
(b) $\alpha = 18$ deg.

Fig. 16. Surface-pressure profiles on airfoil surfaces (for FPBN at $Re = 1.0 \times 10^2$).

low-pressure area over the upstream portion of the upper surface with increasing α and (iv) the leeward expansion of the concentrated high-pressure area just below the fore-face with almost the same peak value of C_p with increasing α. However, we cannot find any features representing the clear discrepancy (v) between $\alpha = 4°$ and $18°$ related with the flow separation on the middle upper surface.

Second, seeing **Fig. 14**, we consider the FP. In **Fig. 14(a)**, we can confirm the features representing the similarities (i) and (ii) without the dependence of α, again. Of course, when we see **Fig. 14(b)**, we can confirm these features, as well as **Fig. 14(a)**. And, when we compare **Figs. 14(a)** and **(b)**, we can confirm the features representing the slight-discrepancies (iii) and (iv), as well as the NACA0015. Again, we cannot find any features representing the clear discrepancy (v).

Third, seeing **Fig. 14**, we compare the NACA0015 and the FP. We can easily find one clear difference between both the airfoils; namely, a sharp and very-low pressure drop near the upper fore-face is seen not for the NACA0015, but for the FP. Besides, we can see another difference between both the airfoils, namely, slightly-higher pressure of the FP than the NACA0015, which is widely-distributed over the middle portion especially of the lower surface. At either α, we see both the sharp pressure drop near the upper fore-face and the higher pressure widely-distributed on the lower surface of the FP. It is reasonable to consider that both the sharp pressure drop and the lower-surface higher pressure of the FP contribute to such superior aerodynamic characteristics as the higher C_L and the higher C_L/C_D of the FP than the NACA0015. We could supposed that the sharp pressure drop is due to sharp leading edges of the FP, and that the lower-surface higher pressure is due to a non-convex lower surface of the FP. Strictly speaking, at $\alpha = 4°$ (in **Fig. 14(a)**), the slightly-lower pressure widely-distributed over the middle portion of the upper surface of the NACA0015 could contribute the improvement of aerodynamic characteristics than the FP, due to a convex upper surface of the NACA0015. However, from a total point of view, the contribution by the slightly-lower pressure on the lower surface of the NACA0015 surpasses that on the upper surface. – We can consider that the sharp pressure drop near the upper fore-face seen only for the FP, which should be ∞ in the thin-airfoil potential theory, is related with the flow along the sharp leading edge of the FP with no separation. This is in consistent with [15] such as "There is no flow separation when $\alpha \leq 10°$. However, when $\alpha = 20°$, the flow begins to separation near the upper leading edge because of the strong local adverse pressure gradient." –

In summary, we can recognise the importance of sharp leading edges for the improvement of aerodynamic characteristics at very low *Re*, which brings the sharp and very-low pressure drop near the upper fore-face. As well, we can recognise the importance of a non-convex lower surface for the improvement, which brings the widely-distributed higher pressure on the lower surface. And, we can also recognise the importance of a convex upper surface for the improvement, which brings the slightly-lower pressure widely-distributed over the middle portion of the upper surface. These three importances just imply the possibilities of the FPBi and the FPBN, and the first and third importances just imply the possibility of the iNACA0015.

Now, seeing **Fig. 14**, we consider the iNACA0015 referring to both the NACA0015 and the FP. In **Fig. 14(a)**, we can confirm (vi) the constant low-pressure area all over the upper surface, instead of (i) the widely-distributed low-pressure area over the upstream portion of the upper surface. That is to say, the upper-surface-pressure profile of the iNACA0015 is close to neither the NACA0015 nor the FP. As the constant pressure of (vi) is not very low but close to zero, the appearance of (vi) suggests inferiority in aerodynamic performance. However, we can confirm (ii) the concentrated high-pressure area just below the fore-face, as well as the NACA0015 and the FP. That is to say, the lower surface-pressure profile of the iNACA0015 is rather close to that of the NACA0015, and its high-pressure area is winder than that for the NACA0015 which suggests superiority in aerodynamic performance. On the other hand, in **Fig. 14(b)** we can confirm that both the profiles on upper and lower surfaces of the iNACA0015 are close to the FP. More strictly, C_p on the downstream portion of the lower surface is rather close to that of the NACA0015.

Next, seeing **Fig. 15**, we consider the FPBi. In **Fig. 15(a)**, we can confirm (vi) the constant-low-pressure are all over the upper surface, as well as the iNACA0015 in **Fig. 14(a)**. However, the lower-surface-pressure profile of the FPBi is close to the FP. In **Fig. 15(b)**, we can confirm that both the profiles on upper and lower surfaces of the FPBi are close to those of the FP, respectively.

Finally, seeing **Fig. 16**, we consider the FPBN. In **Fig. 16(a)**, we can confirm the upper-surface-pressure profile of the FPBN almost coincides with that of the NACA0015, and that the lower-surface-pressure profile of the FPBN almost coincides with that of the FP. In **Fig. 16(b)**, we can confirm these coincidences, again. This seems consistent, if we remind that the FPBN is composed of the upper half of the NACA0015 and the lower half of the FP.

In summary, at very low *Re*, the aerodynamic characteristics of the FPBi, the FPBN and the FP show the best performance, and those of the iNACA0015 are quantitatively superior to those of the NACA0015, but inferior to those of the three best-performance airfoils. This seems consistent, as the three best-performance airfoils have sharp leading edges and non-convex lower-surfaces for the superiority. On the other hand, the iNACA0015 has a sharp leading edge for superiority, and has a convex lower-surface for inferiority. Especially for the aerodynamics of the iNACA0015 and the FPBi at small α, we need further investigations.

4. Conclusions

We have proposed three kinds of two-dimensional airfoils with high performance at low *Re*; namely, the iNACA0015, the FPBi and the FPBN. And, we have investigated them in comparison with such basic airfoils as a NACA0015 and an FP, by two- and three-dimensional computations, at $Re = 1.0 \times 10^2$.

As a result, the flow is completely two-dimensional, even at large attack angle α. We have revealed the effects of α upon various aerodynamic characteristics such as C_D, C_L and C_L/C_D. At such a very low *Re* as 1.0×10^2, the aerodynamic characteristics of all the five airfoils are qualitatively similar with one another. And quantitatively, such three airfoils as the FPBi, the FPBN and the FP show the best performance, which are superior to the NACA0015. The aerodynamic performance of the iNACA0015 is between the three best-performance airfoils and the NACA0015. Among the three best-performance airfoils, the FPBi is supreme. Concerning the controllability, the NACA0015 is superior among the five airfoils, due to the lack of a remarkable stall feature on C_L/C_D. The maximum C_L/C_D is attained by the FPBi at $\alpha = 18°$, and improves by 34% in comparison with the maximum C_L/C_D attained by the NACA0015. This suggests the possibility of more-efficient flights with long ranges in actual operations of UAVs/MAVs. Concerning the controllability, the NACA0015 is superior among the five airfoils, due to the lack of a remarkable stall feature on C_L/C_D. Besides, we have visualised the flow around the airfoils by streamlines and pressure/vorticity distributions around the airfoils at various α's. We have confirmed the consistency between aerodynamic characteristics and the visualised flow, suggesting the importances of sharp leading edges and a non-convex lower surface. Especially for the aerodynamics of the iNACA0015 and the FPBi at small α, we need further investigations.

From a general point of view, the present results imply the gap between the flow at very-low Re and that at ordinary $Re \gtrsim 10^6$. Because the models tested in the present study are restricted, it will be necessary to examine various parameters in the geometry of airfoil's cross section. For example, a concave lower surface, which is common in model plains, might be one promising proposal.

References:

[1] E. N. Jacobs and A. Sherman, "Airfoil Section Characteristics as Affected by Variations in the Reynolds Number," NACA Technical Report, No.586, pp. 227-267, 1937.

[2] I. H. Abbott and A. E. von. Doenhoff, "Theory of Wing Sections," Dover, pp. 462-463, 1958.

[3] F. W. Riegels, "Aerofoil Sections," Butterworths, 1961.

[4] R. Eppler, "Airfoil Design and Data," Springer-Verlag, 1990.

[5] H. Kawano, "Three-Dimensional Obstacle Avoidance of Blimp-Type Unmanned Aerial Vehicle Flying in Unknown and Non-Uniform Wind Disturbance," J. of Robotics and Mechatronics, Vol.19, No.2, pp. 166-173, 2007.

[6] K. Iwata, K. Matsubara, K. Kawasaki, and O. Matsumoto, "Turbojet Engine for Aerial Cargo Robot (ACR)," J. of Robotics and Mechatronics, Vol.24, No.6, pp. 1040-1045, 2012.

[7] J. H. McMasters and M. L. Henderson, "Low Speed Single Element Airfoil Synthesis," Tech. Soaring, Vol.6, pp. 1-21, 1980.

[8] M. Okamoto, K. Yasuda, and A. Azuma, "Aerodynamic Characteristics of the Wings and Body of a Dragonfly," J. of Experimental Biology, Vol.199, pp. 281-294, 1996.

[9] H. Abe, Y. Tutui, and H. Yoshiki, "Aerodynamic Characteristics of an Airfoil in Turbulent and Low-Reynolds-No.Flows: Experiments with a Jet Grid," Trans. of the Japan Society of Mechanical Engineers, Series B, Vol.62, No.602, pp. 3592-3598, 1996 (in Japanese).

[10] S. Sunada, A. Sakaguchi, and K. Kawachi, "Airfoil Section Characteristics at a Low Reynolds Number," Trans. ASME, J. of Fluids Engineering, Vol.199, pp. 129-135, 1997.

[11] H. Abe, "Aerodynamic Characteristics of an Airfoil in Turbulent and Low-Reynolds-No.Flows," Technical Report of Mechanical Engineering Laboratory, AIST, Vol.186, 2000 (in Japanese).

[12] H. Isikawa, D. Kudo, M. Kiya, O. Mochizuki, and Z. Zheng, "Aerodynamic Characteristics of a Flat-Plate Wing with Leading-Edge Serrations," Trans. of the Japan Society of Mechanical Engineers, Series B, Vol.67, No.655, pp. 680-687, 2001 (in Japanese).

[13] T. Motohashi, "Characteristics of Rectangular Wings at Low Reynolds Numbers," Proc. 39th Aircraft Symposium, JSASS, Paper No.3D6, pp. 1-4, 2001 (in Japanese).

[14] N. Nakane, T. Tanaka, and T. Motohashi, "Aerodynamic Characteristics of NACA0012 in a Wide Reynolds No.range," Proc. 35th Fluid Dynamics Conf., JSASS, pp. 179-182, 2003 (in Japanese).

[15] Q. Sun and I. D. Boyd, "Flat-Plate Aerodynamics at Very Low Reynolds Number," J. of Fluid Mechanics, Vol.502, pp. 199-206, 2004.

[16] R. Takagi, "Aerodynamic Characteristics of NACA4402 in Low Reynolds No.Flows," J. of the Japan Society for Aeronautical and Space Sciences, Vol.54, No.631 pp. 367-373, 2006 (in Japanese).

[17] T. Ohtake, Y. Nakae, and T. Motohashi, "Nonlinearity of the Aerodynamic Characteristics of NACA0012 Aerofoil at Low Reynolds Numbers," J. of the Japan Society for Aeronautical and Space Sciences, Vol.55, pp. 439-445, 2007 (in Japanese).

[18] H. Yagi and M. Kawahara, "Optimal Shape Determination of a Body Located in Incompressible Viscous Fluid Flow," Computer Methods in Applied Mechanical and Engineering, Vol.196, pp. 5084-5091, 2007.

[19] E. Katamine, N. Nishihashi, and H. Azegami, "Shape Optimization of Steady-State Viscous Flow Fields for Drag Minimization and Lift Maximization," Trans. of the Japan Society of Mechanical Engineers, Series B, Vol.74, No.748, pp. 2426-2433, 2008 (in Japanese).

[20] T. Ohtake and T. Motohashi, "Flow Field around NACA0012 Airfoil at Low Reynolds Numbers," J. of the Japan Society for Aeronautical and Space Sciences, Vol.57, pp. 397-404, 2009 (in Japanene).

[21] K. Taira and T. Colonius, "Three-Dimensional Flows Around Low-Aspect-Ratio Flat-Plate Wings at Low Reynolds Numbers," J. of Fluid Mechanics, Vol.623, pp. 187-207, 2009.

[22] K. Hirata, M. Kawakita, T. Iijima, M. Koga, M. Kihira, and J. Funaki, "Numerical and Experimental Study on Aerodynamic Characteristics of Basic Airfoils at Low Reynolds Numbers," J. of Fluid Science and Technology, Vol.5, pp. 447-463, 2010.

[23] Y. Zhou, Md. Mahbub Alam, H. X. Yang, H. Guo, and D. H. Wood, "Fluid Forces on a Very Low Reynolds No.Airfoil and Their Prediction," Int. J. of Heat and Fluid Flow, Vol.32, pp. 329-339, 2011.

[24] S. Ebata, T. Yasuda, H. Minagawa, Y. Miyamoto, and N. Satofuka, "A Study of Cross-Sectional Shape of Wing for Underwater Glider at Low Reynolds No.Region," Trans. of the Japan Society of Mechanical Engineers, Series B, Vol.79, No.806, pp. 12-25, 2013 (in Japanene).

Name:
Katsuya Hirata

Affiliation:
Professor, Department of Mechanical Engineering, Doshisha University

Address:
1-3 Tatara Miyakodani, Kyotanabe, Kyoto 610-0321, Japan

Brief Biographical History:

1987- Research Associate, Kyushu University
1993 Received D.E. degree from Kyushu University
1993- Lecturer, Doshisha University
1996- Associate Professor, Doshisha University
2002- Professor, Doshisha University

Main Works:

- "Measurements of Minute Unsteady Pressure on Three-Dimensional Fan with Arbitrary Axis Direction," Int. J. of Fluid Machinery and Systems, Vol.3, pp. 1-10, 2010.
- "On the Critical Submergence for Air-Entraining Vortices in a Suction Sump," Doboku Gakkai Ronbunshu, No.747/II-65, pp. 61-69, 2003.
- "The Aerodynamic Mechanism of Galloping," Trans. of JSASS, Vol.36, pp. 257-269, 1994.
- "Critical Geometry of Oscillating Bluff Bodies," J. of Fluid Mechanics, Vol.208, pp. 375-393, 1988.

Membership in Academic Societies:

- Turbomachinery Society of Japan (TSJ)
- The Japan Society of Mechanical Engineers (JSME)
- Japan Society of Civil Engineers (JSCE)
- The Japan Society for Aeronautical and Space Sciences (JSASS)

Name:
Ryo Nozawa

Affiliation:
Student, Graduate School of Doshisha University

Address:
1-3 Tatara Miyakodani, Kyotanabe, Kyoto 610-0321, Japan

Brief Biographical History:
2011 Received M.E. degree from Doshisha University
2011- Yamaha Motor Engineering Co., Ltd.

Name:
Shogo Kondo

Affiliation:
Student, Graduate School of Doshisha University

Address:
1-3 Tatara Miyakodani, Kyotanabe, Kyoto 610-0321, Japan

Brief Biographical History:
2016 Received M.E. degree from Doshisha University
2016- Aisin Seiki Co., Ltd.

Name:
Kazuki Onishi

Affiliation:
Student, Graduate School of Doshisha University

Address:
1-3 Tatara Miyakodani, Kyotanabe, Kyoto 610-0321, Japan

Brief Biographical History:
2015 Received B.E. degree from Doshisha University
2015- Master Course Student, Doshisha University

Membership in Academic Societies:
- The Japan Society of Mechanical Engineers (JSME)

Name:
Hirochika Tanigawa

Affiliation:
Professor, Department of mechanical Engineering, National Institute of Technology, Maizuru College

Address:
234 Shiroya, Maizuru 625-8511, Japan

Brief Biographical History:
1991- Research Associate, National Institute of Technology, Maizuru College
2000 Received D.E. degree from Doshisha University
2005- Associate Professor, National Institute of Technology, Maizuru College
2011- Professor, National Institute of Technology, Maizuru College

Main Works:
- "Thermal Convection in an Oscillating Cube at Various Frequencies and Amplitudes," Trans. of the Japan Society of Mechanical Engineers, Series B, Vol.79, No.807, pp. 2524-2536, 2013.
- "On the Effect of Forced-Oscillation Amplitude upon the Flow in a Cubic Cavity Heated Below (Fluids Engineering)," Trans. of the Japan Society of Mechanical Engineers, Series B, Vol.75, No.759, pp. 2106-2114, 2009.
- "Sloshing Mode and Finite-Amplitude Effect in Prisms with Rectangular and Triangular Cross Sections," Trans. of the Japan Society of Mechanical Engineers, Series B, Vol.69, No.684, pp. 1854-1861, 2003.
- "Vibrational Effects on Convection in a Square Cavity at Zero Gravity," J. of Fluid Mechanics, Vol.445, pp. 327-344, 2001.

Membership in Academic Societies:
- The Japan Society of Mechanical Engineers (JSME)